Inclusion of chemical effect in a fully coupled THM finite element code

A.A. Abed & W. Sołowski
Department of Civil Engineering, Aalto University, Finland

E. Romero & A. Gens
Departamento de Ingenieria del Terreno, Universitat Politecnica de Catalunya, Spain

ABSTRACT: Bentonite-rich clays can be used as a buffer / backfill material in deep geological repositories for nuclear waste. The prediction of the long-term performance of a buffer / backfill in such a complex environment, where the temperature, humidity and chemistry of water change, requires a fully thermo-hydro-mechanical-chemical (THMC) coupled numerical code. This paper presents a simple extension of a THM coupled finite element code to include chemical effects. After deriving the governing salt mass balance equation and discussing its implementation into the code, the paper verifies the extended framework against an analytical solution for 1D salt transport. In addition, the article presents a validation example in which the code replicates experimental data. The numerical results obtained from the extended THMC coupled finite element code encourage further investigation of the chemical effects on the mechanical and thermal behaviour of the material, which would serve the ultimate goal of achieving a safer design of the nuclear waste storage facility.

1 INTRODUCTION

The salt concentration in pore water affects significantly the behaviour of bentonite-rich clays which are used for creating highly impervious barriers, useful, for example, in construction of geological storage for nuclear waste. Salts affect the microstructure of those clays, resulting in altering the mechanical properties, permeability and heat conductivity. In particular, the swelling pressure, crucial for keeping the barrier intact, reduces with increasing salt concentration. Therefore, safe design of the buffer and backfill in the storage requires considering effects of salt on the barrier material.

This contribution introduces a simple chemical coupling into the current theoretical and numerical framework of thermo-hydro-mechanical coupled Aalto Finite Element code (Abed & Sołowski 2017). The paper starts with a brief explanation of the solved governing balance equations. In particular, the salt mass balance equation is explained in detail as it represents the new development in the code. Subsequently the paper presents two benchmark examples, which verify and validate the introduced chemical coupling. The comments and outlook on the possible future developments follow.

2 GOVERNING BALANCE EQUATIONS

2.1 *Mass balance*

The paper adopts the compositional method to derive the components balance equations (Olivella et al. 1996; Panday & Corapcioglu 1989). Upon considering the salt as an additional component in the geomaterial representation, one ends up with four distinct components: 1) water (w) being in liquid and/or vapour state; 2) dry air (a) being in the voids or dissolved in liquid phase; 3) salt (st) being in solid state or dissolved in liquid phase and 4) solid component (s) representing the geomaterial. The general mass balance equation is (Abed & Sołowski 2017):

$$\underbrace{\frac{\partial\left(\phi^i\rho^i\omega_k^i\right)}{\partial t}}_{storage}+\underbrace{\boldsymbol{\nabla}\cdot\left(\phi^i\rho^i\omega_k^i\boldsymbol{v}^i\right)}_{advection}+\underbrace{\boldsymbol{\nabla}\cdot\boldsymbol{j}_k^i}_{non-advection}=\underbrace{Q_k^i}_{sink/source} \tag{1}$$

where the symbols ϕ^i and ρ^i denote volume fraction and density of the phase i (*i=solid (s),liquid (l), gas (g)*). The mass fraction of component k in the i-phase is expressed by $\omega_k^i=\rho_k^i/\rho^i$. The phase-velocity vector is represented by $\boldsymbol{v}^i$ whereas $\boldsymbol{j}_k^i$ is the non-advective flux vector of the component k. The term Q_k^i represents any internal or external mass source or sink in the studied domain. For a full discussion on Equation 1 and detailed explanation of the constitutive assumptions used in the developed framework

see (Abed & Sołowski 2017). Here, to avoid repetition and due to space limitation, only the new salt component mass balance equation will be discussed.

2.1.1 *Salt component balance equation*

The salt component can be found as dissolved in liquid phase or crystallised (adsorbed) in the solid phase. Accordingly, the general salt mass balance equation is established by summing the contributions coming from these two parts. For the *salt in the solid phase*, Equation 1 is written as:

$$\frac{\partial(\phi^s \rho^s \omega_{st}^s)}{\partial t} + \boldsymbol{\nabla} \cdot (\phi^s \rho^s \omega_{st}^s \boldsymbol{v}^s) + \boldsymbol{\nabla} \cdot \boldsymbol{j}_{st}^s = Q_{st}^s \tag{2}$$

Equation 2 does not take into account any chemical reactions in which salt may take part, which could affect the mass balance.

Similarly, for the *dissolved salt in the liquid phase*, Equation 1 yields:

$$\frac{\partial(\phi^l \rho^l \omega_{st}^l)}{\partial t} + \boldsymbol{\nabla} \cdot (\phi^l \rho^l \omega_{st}^l \boldsymbol{v}^l) + \boldsymbol{\nabla} \cdot \boldsymbol{j}_{st}^l = Q_{st}^l \tag{3}$$

Noticing the condition $Q_{st}^s = -Q_{st}^w$ which means that any adsorbed salt should result in an equal loss in dissolved salt mass and vice versa, summing Equations 2 and 3 eventually yields the governing salt mass balance equation:

$$\frac{\partial\big((1-n)\rho^s C_s\big)}{\partial t} + \frac{\partial(nS^l C)}{\partial t} + \boldsymbol{\nabla} \cdot (q^l C) + nS^l D_h \nabla \cdot C = 0, \tag{4}$$

where ρ^s is the solid particles density. The dispersion coefficient D_h reflects both molecular diffusion and mechanical dispersion, where:

$$D_h = \tau D_o + \alpha|v|; \quad v = \frac{q^l}{nS^l} \tag{5}$$

The symbols τ, D_o, α, v, q^l, n and S^l represent tortuosity, molecular diffusion coefficient, dispersivity, average liquid velocity, Darcian velocity, porosity and liquid degree of saturation, respectively. The adsorbed concentration (amount of salt per unit mass of solids) C_s (mol/kg) is assumed to correlate linearly with the dissolved concentration C (mol/l) through a distribution coefficient K_d(l/kg) where $C_s = K_d C$.

It is worth mentioning that Equation 4 is derived neglecting any mechanical deformations which is a strong assumption in the case of swelling materials similar to bentonite. It also does not consider the changes in the solid phase density and the liquid phase density due to salt concentration. An improved version of Equation 4 is planned to be soon incorporated in the code.

2.2 *Energy balance equation*

The thermal energy balance equation is satisfied by satisfying the balance of enthalpy:

$$\underbrace{\frac{\partial \Phi_h}{\partial t}}_{Heat\ storage} + \underbrace{L Q_w^g}_{latent\ heat\ of\ vaporization} + \underbrace{\nabla \cdot \boldsymbol{q}_h}_{heat\ due\ to\ conduction\ and\ convection} = 0 \tag{6}$$

where the soil heat capacity Φ_h represents the ability of the geomaterial to store or lose heat. The energy released during phase transition is captured by the latent heat of water vaporization L and the rate of vapour production Q_w^g. The flux $\boldsymbol{q}_h$ includes contributions due to heat conduction and convection by liquid and gas phases.

The current formulation does not consider the consequences of energy evolution during phase transition of salt from dissolved state to solid state and the effects of possible chemical reactions on energy balance. It also assumes that the heat storage and heat transport are not affected by the adsorbed salt – an assumption which is going to be revisited in the future developments.

2.3 *Mechanical balance equation*

The net stress $\boldsymbol{\sigma}$ and matric suction s are adopted as two independent stress measures. The mechanical equilibrium is achieved through the classical equation:

$$\nabla \cdot \boldsymbol{\sigma^{tot}} + \boldsymbol{b} = 0 \tag{7}$$

The vector $\boldsymbol{b}$ contains the contribution of stresses due to body forces (gravity for example). The total stress $\boldsymbol{\sigma^{tot}} = \boldsymbol{\sigma} + P_g$ where the pore gas pressure P_g is replaced by pore liquid pressure P_l at full saturation allowing to recover the Terzaghi's definition of effective stress. Matric suction is defined as the difference between gas pressure and liquid pressure, reducing to zero at full saturation.

During the nonlinear calculations, stress integration is needed to be conducted over the loading step. To achieve that, a suitable mechanical constitutive model that accounts for unsaturated geomaterial behaviour should be employed. In this framework, a modified version of the elastoplastic Barcelona Basic Model (Alonso et al. 1990) that accounts for thermal effects (Gens 1995; Laloui & Cekerevac 2003) is implemented.

As this contribution only concentrates on hydrochemical coupling, no more discussion is given to the thermal energy nor to the mechanical component of the code. However, the interested reader in all the details is strongly recommended to consult the contribution (Abed & Sołowski 2017).

3 NUMERICAL IMPLEMENTATION

The salt mass balance equation 4 is discretised using the finite element method where the primary unknown is the nodal salt concentration $\hat{c}$. At this stage of the development, the resulted ordinary differential

equation of first order with respect to time is *weakly coupled* to the already established mechanical, thermal and hydraulic parts of the Code. In the sense that the effect of salt concentration on the mechanical behaviour is not yet introduced. To achieve that, one needs to include osmotic suction effects, which are not considered yet in this work. In addition, the mass balance equations of the solid and water components, in its current formulation, do not consider the variation in density and porosity due to salt existence (Alonso et al. 1999; Della Vecchia & Musso 2016; Navarro et al. 2017; Olivella et al. 1996; Sánchez et al. 2016).

The coupled set of first order ordinary differential equations is written as:

$$\boldsymbol{M\dot{X}} + \boldsymbol{KX} = \boldsymbol{F} \tag{8}$$

where $\boldsymbol{M}$, $\boldsymbol{K}$ and $\boldsymbol{F}$ are the mass matrix, stiffness matrix and vector of imposed boundary conditions, respectively. The unknowns are stored in $\boldsymbol{X} = \{\hat{\boldsymbol{u}}, \hat{\boldsymbol{h}}_w, \hat{\boldsymbol{h}}_g, \hat{\boldsymbol{T}}, \hat{c}\}$, representing the nodal displacements, pore water pressure head, pore gas pressure head, temperature and salt concentration, respectively.

These equations are discretised further with respect to time using finite differences method to produce a set of nonlinear algebraic equations, which is solved using Newton-Raphson iterations. Knowing the initial conditions at time step i, the residual $\boldsymbol{R^{i+1}}$ at the time step $i+1$ is:

$$\boldsymbol{R}^{i+1} = \boldsymbol{M}^{i+1}\frac{\boldsymbol{X}^{i+1} - \boldsymbol{X}^{i}}{\Delta t} + \boldsymbol{K}^{i+1}\boldsymbol{X}^{i+1} - \boldsymbol{F}^{i+1} \tag{9}$$

The solution is considered to be converged once the Euclidean norm of the residual is reduced below a desired tolerable error $\|R\| < Tol$.

This formulation is implemented into a FE code using NUMERRIN numerical solver (Laitinen 2013). The implementation includes special logical switches coded which allow to choose the balance equations to be coupled in Equation 8 and used in the subsequent formation of residuals in Equation 9.

4 NUMERICAL EXAMPLES

4.1 *Verification of 1D salt transport*

The analytical solution by (Lapidus & Amundson 1952) for 1D salt transport is used to verify the implementation of the corresponding equation as introduced in Section 2.1.1. For that purpose, only the coupled solution of water mass balance equation and salt mass balance equation are activated. According to Lapidus & Amundson (1952), if a soil is subjected to salt concentration C_o at the surface, then the concentration of salt at a depth z and time t equals:

$$C(z,t) = \frac{C_o}{2}\left[\operatorname{erfc}\left(\frac{R_d z - vt}{\sqrt{4R_d D_h t}}\right) + \mathrm{e}^{\left(\frac{vz}{D_h}\right)}\operatorname{erfc}\left(\frac{R_d z + vt}{\sqrt{4R_d D_h t}}\right)\right] \tag{10}$$

where erfc is the complementary error function being defined as:

$$\operatorname{erfc}(x) = \frac{2}{\sqrt{\pi}}\int_x^{\infty} \mathrm{e}^{-t^2} dt \tag{11}$$

where e is the Napier's constant. The R_d term is given as:

$$R_d = 1 + \frac{(1-n)\rho^s K_d}{nS^l} \tag{12}$$

4.1.1 *Finite element model*

The employed finite element mesh is illustrated in Figure 1(a). It consists of 300 4-noded elements with 4 Gauss integration points per element. The mesh is chosen after a careful convergence and mesh sensitivity study. The hydraulic and chemical boundary conditions are depicted in Figure 1.

By neglecting the gravitational effect and assuming a saturated hydraulic conductivity of $K_{sat} = 1.0\ m/s$, the hydraulic boundary conditions are chosen in a way that a constant Darcian velocity of $q^l = 0.5\ m/s$ is generated in the whole solved domain. The geomaterial is considered to be fully saturated with $S^l = 1.0$ and its porosity $n = 0.5$. These assumptions result in an average velocity:

$$v = \frac{q^l}{nS^l} = \frac{0.5}{0.5\times 1.0} = 1.0\ m/s$$

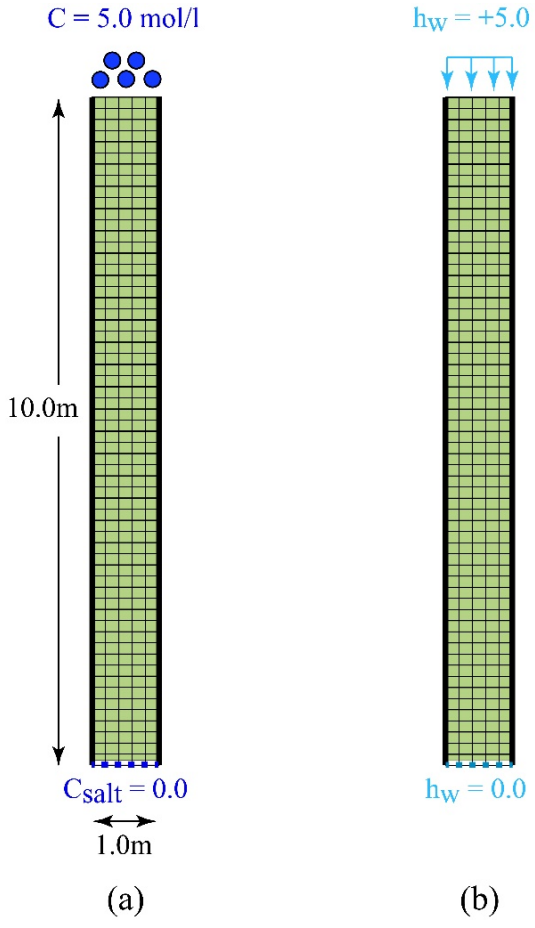

Figure 1. Finite element model: a) mesh, geometry and chemical boundary conditions; b) hydraulic boundary conditions.

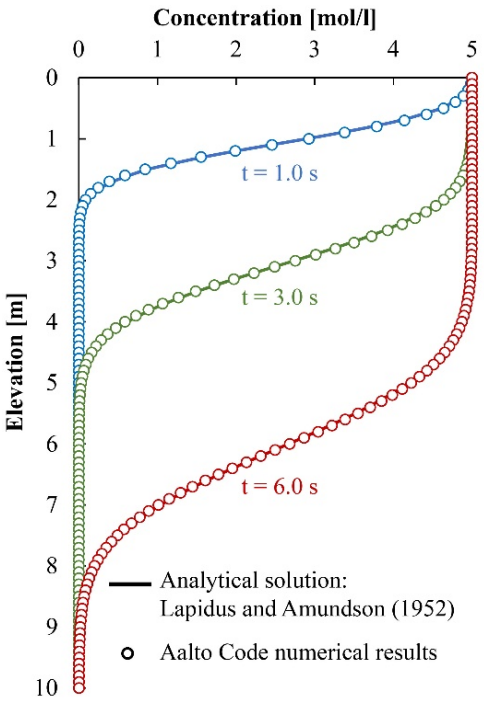

Figure 2. Numerical results versus analytical solution.

No salt adsorption is considered to take place, that is achieved by assuming $K_d = 0$ resulting in $R_d = 1.0$.

Initially, the material has zero salt concentration $C(z,0) = 0.0$. For $t > 0.0$ a salt concentration $C = 5.0\, mol/l$ is prescribed at the top boundary while keeping the bottom at zero concentration. The chemical boundary conditions are shown in Figure 1(a). The total simulated time is 10.0 seconds.

4.1.2 *Calculation results*

Figure 2 shows a perfect match between the numerical results and the analytical solution at different time steps ($t = 1.0\, s$, $3.0\, s$ and $6.0\, s$). The calculation results verify the correctness of the implementation of the transport equations 1 and 4 in the Aalto Code.

4.2 *Validation of coupled liquid-salt movement*

Warrick et al. (1971) performed a field infiltration experiment where an unsaturated homogeneous soil was exposed to simultaneous infiltration of water and salt (chloride) at its surface. The initial salt concentration of $209.0\, meq/l$ ($0.209\, mol/l$) was imposed for the first 168.0 minutes (0.1167 day) before it dropped to zero for the rest of experiment duration. The soil water content and salt concentration at different soil depths and time steps of the test duration were measured and made available for the purposes of numerical modelling. Many researchers used this well-controlled experiment to validate their numerical schemes including (Boufadel et al. 1997; Bresler & Hanks 1969; Gureghian et al. 1979; Ungs et al. 1976; Van Genuchten 1982). Beside the recorded experimental data, the obtained numerical results by Van Genuchten (1982) and Boufadel et al. (1997) will be used as reference in this example to judge on the validity of the mathematical framework.

The water retention curve of the soil was derived to fit the experimental data and is given as (Warrick et al. 1971):

$$\begin{aligned} &\text{if } \psi > 0.295\, m \\ &\qquad S^l = 0.6378 - 0.2506\, \mathrm{Ln}(\psi) \\ &\text{else} \\ &\qquad S^l = 0.86 - 0.0719\, \mathrm{Ln}(\psi) \end{aligned} \tag{13}$$

where ψ is the suction head. Similarly, the relative permeability curve is given as (Warrick et al. 1971):

$$K_{rel} = 1.2354 \times 10^{-6} \times e^{13.604 \times S^l} \tag{14}$$

thus, the actual hydraulic conductivity at any degree of saturation can be estimated as $K = K_{rel} K_{sat}$. The performance of both Equation 13 and Equation 14 in fitting the experimental data is graphically shown in Figure 3. A maximum value of 1.0 is imposed on the resulted values of S^l and K_{rel} in Equations 13 and 14.

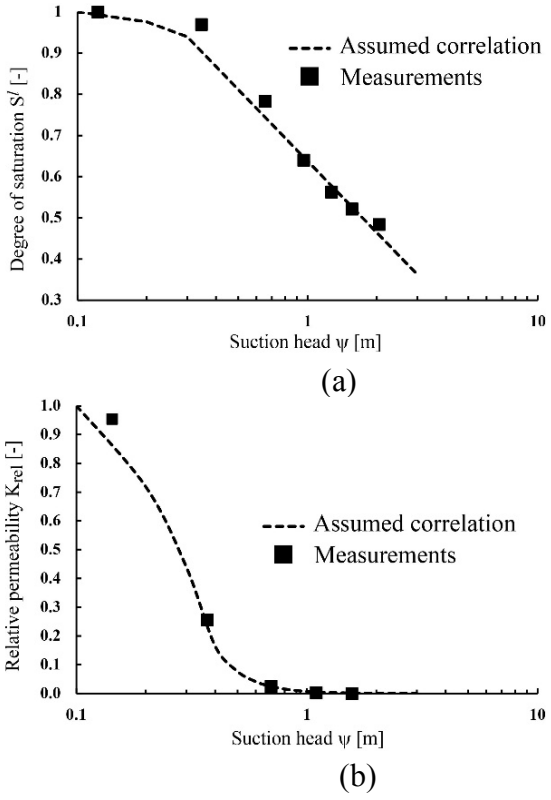

Figure 3. Performance of the employed water retention formula (a) and relative permeability function (b) in fitting the experimental data.

Table 1. Relevant soil properties.

Index property	
Water flow	
Saturated hydraulic conductivity K_{sat} (m/s)	4.456e-06
Salt transport	
Molecular diffusion coefficient τD_o (m^2/s)	6.94e-10
Dispersivity α (m)	0.01
Distribution coefficient K_d (l/kg)	0.0
Others	
Porosity n (-)	0.38

The initial suction profile is derived based on the measured initial water content as given in Figure 5. The diffusion coefficient and dispersivity are given by Van Genuchten (1982) and are listed in Table 1 together with some other relevant soil properties.

4.2.1 *Finite element model and boundary conditions*

The employed finite element mesh and problem geometry are depicted in Figure 4(a). The converged mesh consists of 500 4-noded elements. The initial salt concentration is zero.

The experiment is simulated for 10.0 hours and the results are discussed for time steps t = 2.0 hr and t = 9.0 hr.

4.2.2 *Volumetric water predictions*

The volumetric water content $\theta = nS^l$ profile as predicted by Aalto Code is shown in Figure 5. The figure also includes the measured data and reference calculations by Boufadel et al. (1997) and Van Genuchten (1982). The very good agreement between the prediction and the experimental data at one hand and the perfect match with the reference solutions validate the predictive capabilities of the hydraulic part of the code under similar conditions.

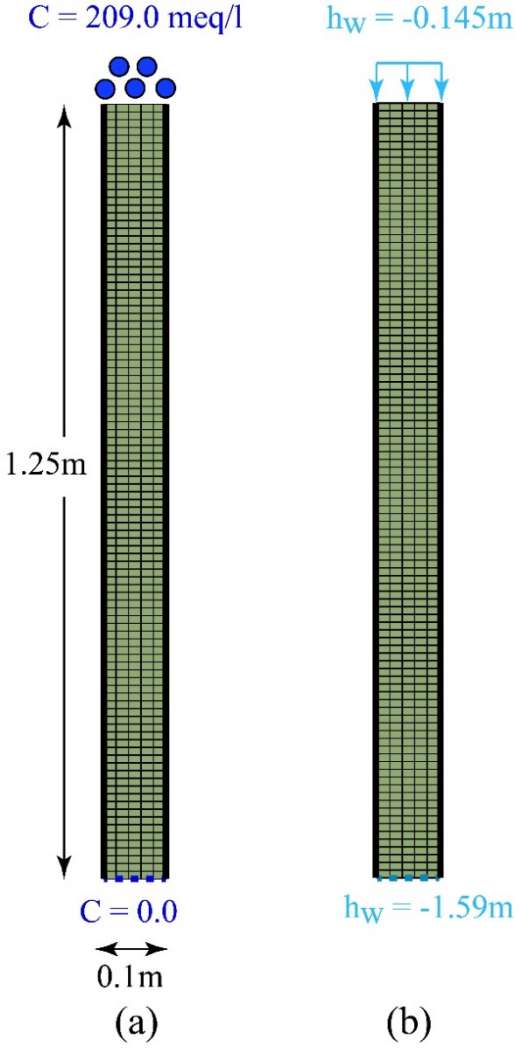

Figure 4. Finite element model: a) mesh, geometry and chemical boundary conditions; b) hydraulic boundary conditions.

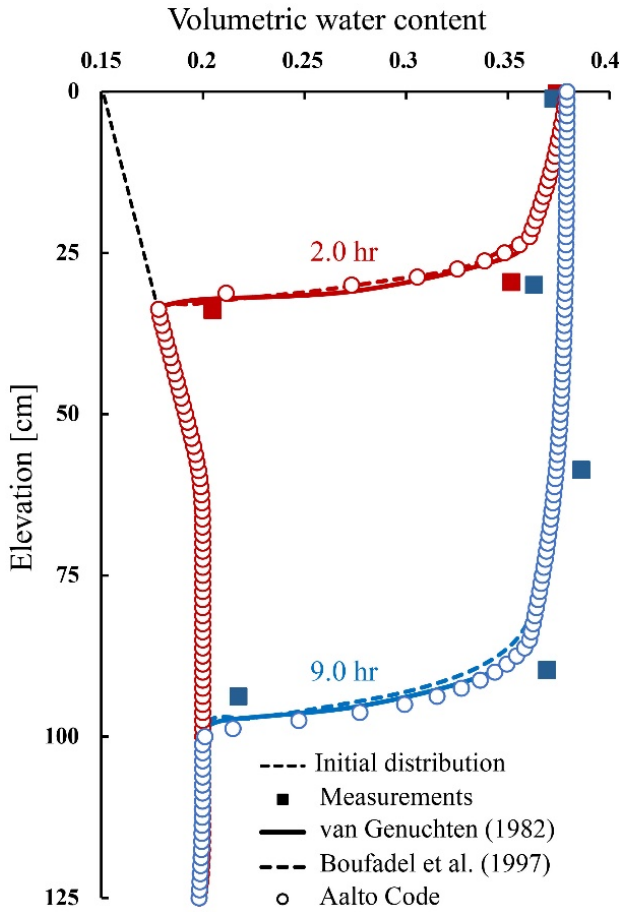

Figure 5. Predicted volumetric water content at t = 2.0 hr and t = 9.0 hr compared to experimental and reference results.

4.2.3 *Salt concentration predictions*

The predicted salt concentration after 2.0 and 9.0 hours are reported in Figure 6. Even though the Aalto Code numerical prediction fits very well the reference solutions, yet there is still appreciable difference between the numerical predictions and the actual field measurements. This was attributed by Warrick et al. (1971) to the possible lack of complete salt mixing within all soil pores as the biggest amount of water moves through the larger pore.

This benchmark provides partial validation of the code with respect to salt transport prediction.

5 CONCLUSIONS

This paper presents an extension of the coupled THM Aalto Code to include the capability to predict salt concentration evolution in time. The article introduces the mass balance equation of salt based on the compositional method into other existing mass balance equations. The implementation is then verified against analytical solution and partially validated against available experimental data.

To obtain the predictive capability of the framework, further developments are necessary. Those include better chemical coupling with the mechanical part of the code, considering the effect of possible salt

crystallization on the thermo-hydro-mechanical behaviour of unsaturated geomaterials as well as the effects of salt concentration on material microstructure, permeability and heat transport properties.

The ultimate target is to improve the accuracy of numerical predictions of the complex coupled THMC behaviour of clay under extreme environmental conditions such as those encountered by the material when used as a sealing material for spent nuclear fuel. That would eventually be reflected in a safer and more sustainable design of the engineering barrier.

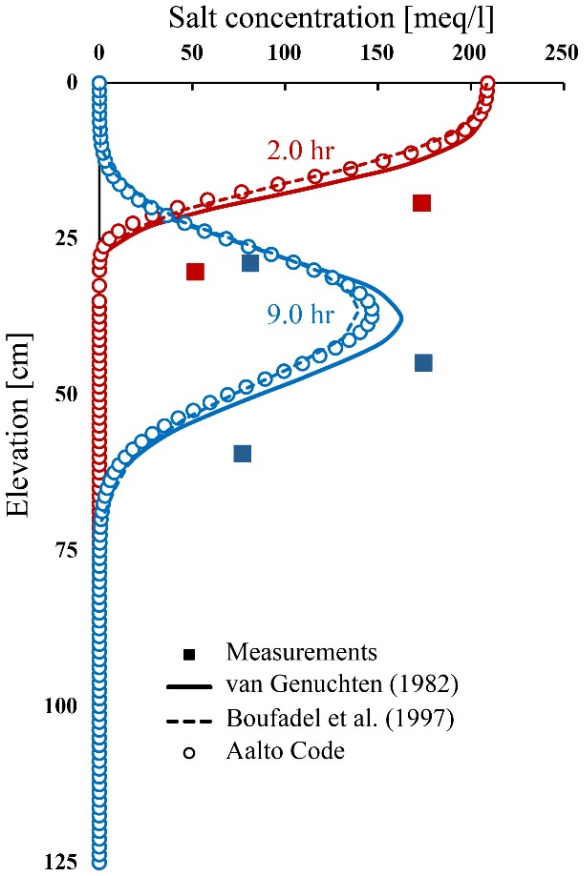

Figure 6. Predicted salt concentration at t=2 hr and t=9 hr compared to experimental and reference results.

6 ACKNOWLEDGEMENTS

The authors would like to gratefully acknowledge that the presented research has been funded by KYT2018 Finnish Research Programme on Nuclear Waste Management via THEBES project.

7 REFERENCES

Abed, A. A., & Sołowski, W. T. 2017. A study on how to couple thermo-hydro-mechanical behaviour of unsaturated soils: Physical equations, numerical implementation and examples. *Computers and Geotechnics* 92: 132-155.

Alonso, E. E., Gens, A., & Josa, A. 1990. A constitutive model for partially saturated soils. *Géotechnique* 40(3): 405-430.

Alonso, E. E., Vaunat, J., & Gens, A. 1999. Modelling the mechanical behaviour of expansive clays. *Engineering geology* 54(1): 173-183.

Boufadel, M. C., Suidan, M. T., & Venosa, A. D. 1997. Density-dependent flow in one-dimensional variably-saturated media. *Journal of hydrology* 202(1): 280-301.

Bresler, E., & Hanks, R. J. 1969. Numerical method for estimating simultaneous flow of water and salt in unsaturated soils. *Soil Science Society of America Journal* 33(6): 827-832.

Della Vecchia, G., & Musso, G. 2016. Some remarks on single- and double-porosity modeling of coupled chemo-hydro-mechanical processes in clays. *Soils and Foundations* 56(5): 779-789.

Gens, A. 1995. Constitutive laws. In *Modern issues in non-saturated soils* (pp. 129-158). Springer Vienna.

Gureghian, A. B., Ward, D. S., & Cleary, R. W. 1979. Simultaneous transport of water and reacting solutes through multilayered soils under transient unsaturated flow conditions. *Journal of Hydrology* 41(3-4): 253-278.

Laitinen, M. 2013. *Numerrin 4.0 Manual*. Numerola Oy: Jyväskylä.

Laloui, L., & Cekerevac, C. 2003. Thermo-plasticity of clays: an isotropic yield mechanism. *Computers and Geotechnics* 30(8): 649-660.

Lapidus, L., & Amundson, N. R. 1952. Mathematics of adsorption in beds. VI. The effect of longitudinal diffusion in ion exchange and chromatographic columns. *The Journal of Physical Chemistry* 56(8): 984-988.

Navarro, V., Yustres, Á., Asensio, L., De la Morena, G., González-Arteaga, J., Laurila, T., & Pintado, X. 2017. Modelling of compacted bentonite swelling accounting for salinity effects. *Engineering Geology* 223: 48-58.

Olivella, S., Carrera, J., Gens, A., & Alonso, E. E. 1996. Porosity variations in saline media caused by temperature gradients coupled to multiphase flow and dissolution/precipitation. *Transport in Porous Media* 25(1): 1-25.

Olivella, S., Gens, A., Carrera, J., & Alonso, E. E. 1996. Numerical formulation for a simulator (CODE_BRIGHT) for the coupled analysis of saline media. *Engineering computations* 13(7): 87-112.

Panday, S., & Corapcioglu, M. Y. 1989. Reservoir transport equations by compositional approach. *Transport in Porous Media* 4(4): 369-393.

Sánchez, M., Gens, A., Villar, M. V., & Olivella, S. 2016. Fully Coupled Thermo-Hydro-Mechanical Double-Porosity Formulation for Unsaturated Soils. *International Journal of Geomechanics* 16(6): D4016015.

Ungs, M., Cleary, R. W., Boersma, L., & Yingjajaval, S. 1976. The description of transfer of water and chemicals through soils. *Land as a Wast Management Alternative (Ed. Loehr, RC), Ann Arbor Science, Ann Arbor*.

Van Genuchten, M. T. 1982. A comparison of numerical solutions of the one-dimensional unsaturated—saturated flow and mass transport equations. *Advances in Water Resources* 5(1): 47-55.

Warrick, A. W., Biggar, J. W., & Nielsen, D. R. 1971. Simultaneous solute and water transfer for an unsaturated soil. *Water Resources Research* 7(5): 1216-1225.